Stem Cell Reports, Volume *16*

Supplemental Information

CRISPR/Cas9/AAV9-mediated *in vivo* editing identifies MYC regulation of 3D genome in skeletal muscle stem cell

Liangqiang He, Yingzhe Ding, Yu Zhao, Karl K. So, Xianlu L. Peng, Yuying Li, Jie Yuan, Zhiming He, Xiaona Chen, Hao Sun, and Huating Wang

Supplemental Information

List of Supplemental Figures

List of Supplemental Tables

Supplemental Experimental Procedures

Supplemental References

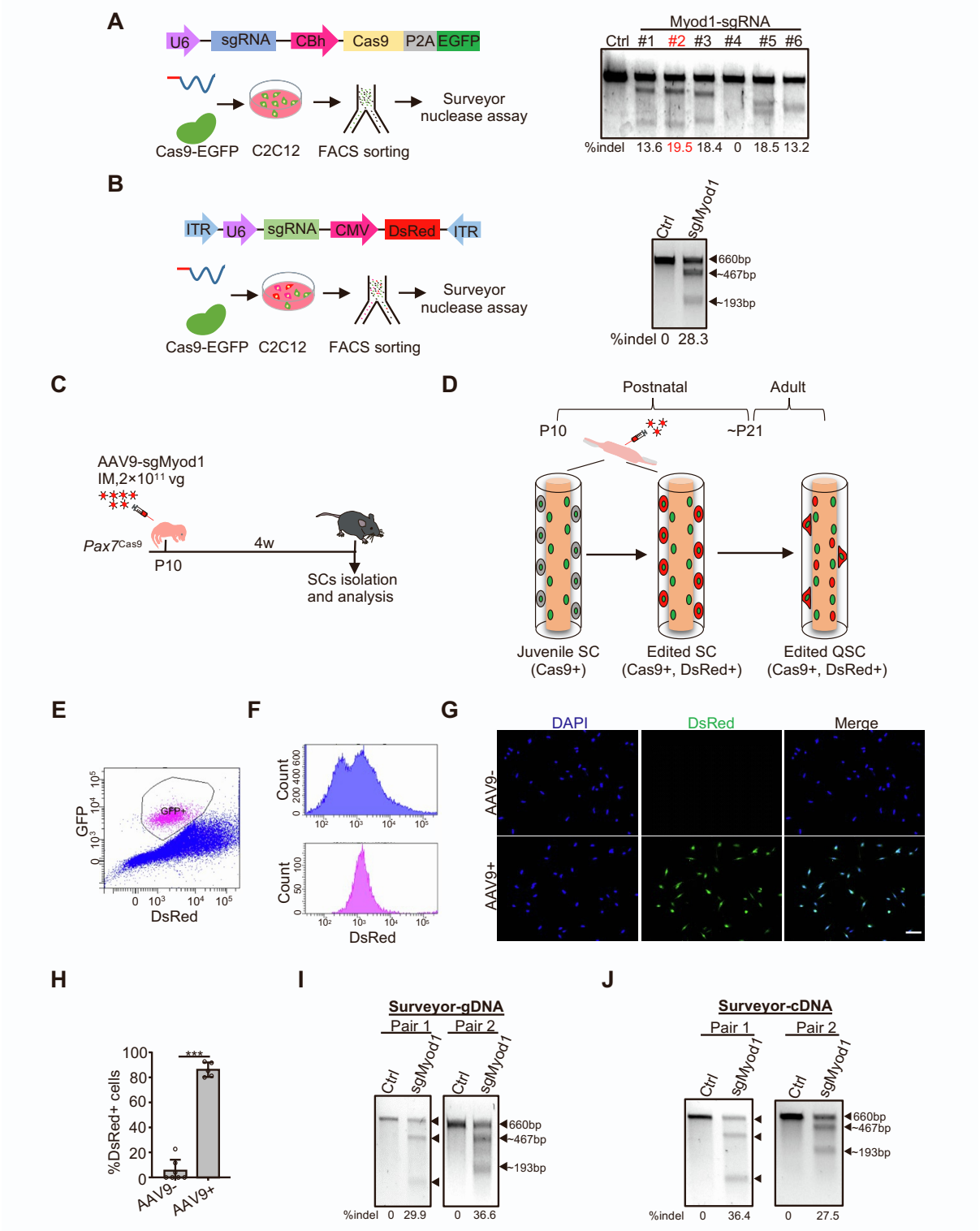

Figure S1. CRISPR/Cas9 in conjunction with AAV9 mediated sgRNAs delivery yields robust editing in juvenile SCs. Related to Figure 2. (**A**) Left: schematic illustration of the sgRNA-Cas9 expressing vector (Upper panel) and the *in vitro* sgRNA selection assay (Lower panel). SgRNA-Cas9 expressing plasmid was transfected into C2C12 myoblasts; positively transfected cells were sorted out by GFP expression one day after transfection and cultured for another two days before Surveyor nuclease assay. Right: agarose gel image showing the result of Surveyor nuclease assay on *Myod1* locus. The percentage of indel formation is shown. SgRNA2 with the highest frequency of indel

formation is indicated in red. (**B**) Testing of AAV9-Myod1-sgRNA2 vector in C2C12 myoblasts. SgRNA2 was cloned in the AAV9-sgRNA vector and transfected into C2C12 cells together with a Cas9-EGFP expressing plasmid (pX458). Positively transfected cells were FACS isolated based on GFP and DsRed expression and cultured for another two days before Surveyor nuclease assay. AAV9-sgRNA backbone without sgRNA insertion was used as a control. Wild type (660 bp) and cleaved bands (~467 bp/193 bp) by Surveyor are indicated by arrowheads. The percentage of indel formation is shown. (**C**) Schematic illustration of the experimental design for AAV administration and SC isolation & analysis. (**D**) Diagram to show the strategy of CRISPR/Cas9/AAV9 mediated *in vivo* editing of *Myod1* in juvenile SCs. AAV9-sgMyod1 virus was intramuscularly (IM) injected into the *Pax7*^{Cas9} mice at P10 to edit the juvenile SCs actively proliferating during the postnatal myogenesis. Upon the termination of the postnatal myogenesis around P21, a portion of the edited cells was expected to return quiescence carrying the editing. (**E**) FACS plot showing the gating strategy to sort out SCs from *Pax7*^{Cas9} mice based on GFP signal four weeks after AAV9-sgMyod1 virus injection. (**F**) Histogram to show the DsRed signal (Upper panel) for all the input cells in Figure S1E. The isolated Cas9-GFP+ SCs were located in the DsRed high population (Lower panel). (**G-H**) FISCs from the AAV9 injected mice were seeded for 24 hrs and IF stained for DsRed (G). SCs from *Pax7*^{Cas9} mice without AAV9 virus infection (AAV9-) were used as a control. The percentage of DsRed positive cells was quantified from at least five randomly selected fields (H). Scale bar, 50 μm. The bar graph presents mean ± s.d. ***P<0.001. (**I**) Genomic DNAs (gDNA) from FISCs of the *Pax7*^{Cas9} mice administrated with AAV9-sgMyod1 viruses were subject to Surveyor assay to test the frequency of indel formation at *Myod1* locus. Wild type (660 bp) and cleaved bands (~467 bp/193 bp) by Surveyor are shown by arrowheads. The percentage of indel formation is shown. n = 2 mice per group. (**J**) SCs isolated from the above mice were cultured for four days and *Myod1* transcripts were subject to Surveyor assay to test the frequency of indel formation at *Myod1* locus. Wild type (660 bp) and cleaved bands (~467 bp/193 bp) by Surveyor are shown by arrowheads. The percentage of indel formation is shown. n = 2 mice per group.

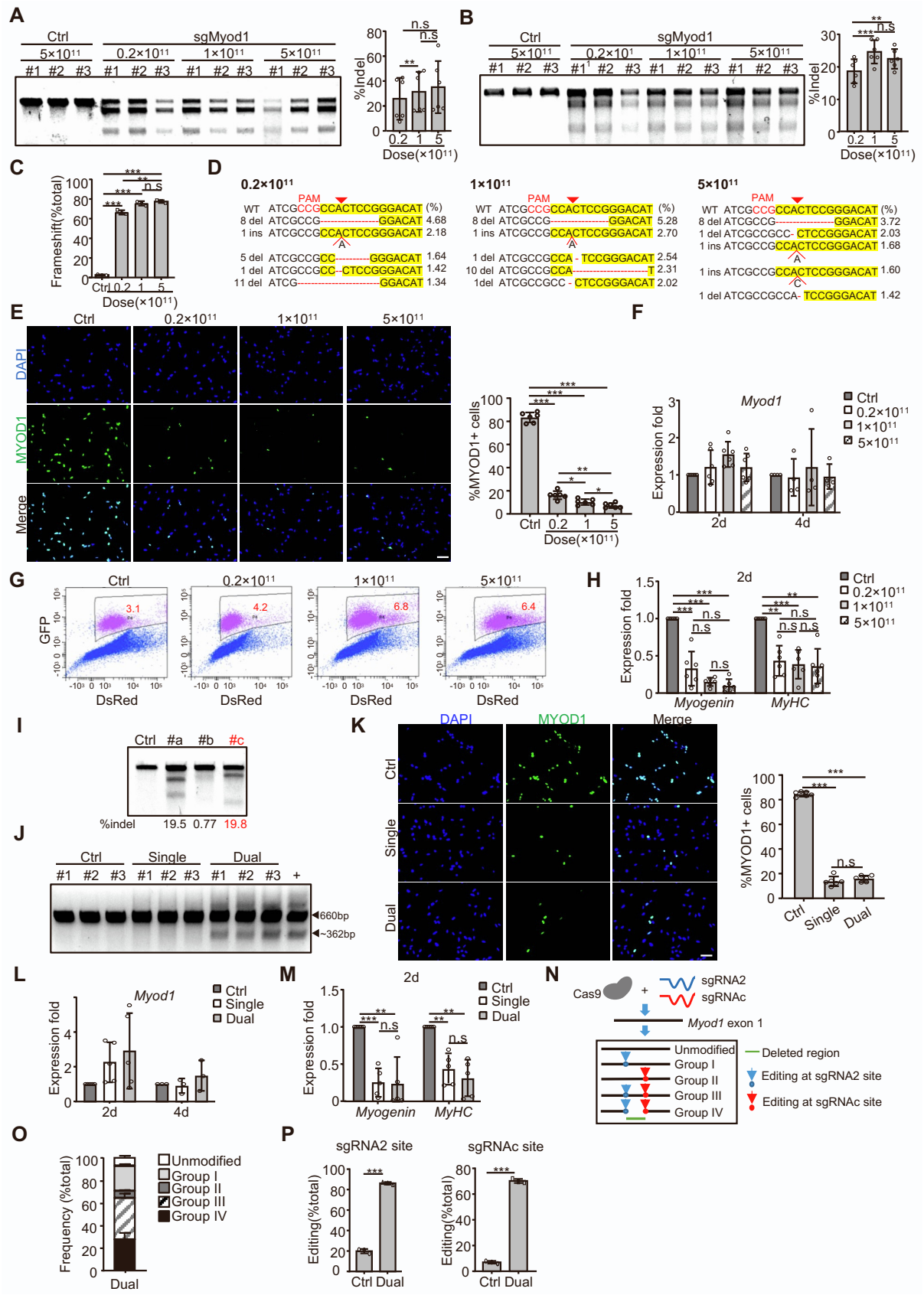

Figure S2. Effect of AAV9 dosage and dual sgRNAs on the CRISPR/Cas9 mediated genome editing in juvenile SCs. Related to Figure 2. (**A**) Left: Genomic DNAs from SCs of *Pax7*^{Cas9} mice administrated with different doses of AAV9-sgMyod1 virus were subject to Surveyor assay to test the

frequency of indel formation at *Myod1* locus. Right: The percentage of indel formation was quantified. n = 6 mice per group. (**B**) Left: SCs isolated from *Pax7*^{Cas9} mice administrated with different doses of the AAV9-sgMyod1 viruses were cultured for two days and Surveyor assay was performed to examine the editing efficiency in *Myod1* transcripts. Right: the indel occurrence was estimated. n = 6 mice per group. (**C**) Quantification of the frameshift mutations determined by deep sequencing of the genomic DNAs from SCs of the *Pax7*^{Cas9} mice administrated with different doses of AAV9-sgMyod1 viruses. The percentage was calculated as the ratio of frameshift mutations to the total reads and presented as mean ± s.d. n = 3 mice per group. (**D**) The five most frequently detected indel classes under each dose of AAV9-sgMyod1 virus are shown. The percentage is calculated as the ratio of reads for each indel class to the total edited reads. The indels included small deletions and +1 bp insertion at target site and the patterns were similar among different doses, which is in agreement with a prior report showing that the repair outcomes of CRIPSR/Cas9 mediated genome editing are not random (van Overbeek et al., 2016). (**E**) Left: the above SCs were cultured for two days and IF stained for MYOD1 protein. Right: the number of positively stained cells was counted. n = 6 mice per group. For each mouse, an average of 9 randomly selected fields were quantified. Scale bar, 50 μm. (**F**) The above SCs were cultured for two or four days and *Myod1* mRNA expression was detected by qRT-PCR (n = 4 to 6 mice per group). (**G**) Representative FACS plots showing the percentage of GFP+ SCs (indicated as red) isolated from *Pax7*^{Cas9} mice administrated with different doses of AAV9-sgMyod1 viruses. (**H**) The above isolated SCs were cultured for two days and the relative expression of *Myogenin* or *MyHC* was detected by qRT-PCR. n = 6 mice per group. (**I**) *In vitro* screening of sgRNAs targeting downstream of *Myod1* exon 1 by Surveyor nuclease assay in C2C12 myoblasts. The percentage of indel formation is presented. SgRNAc selected for *in vivo* study is marked in red. (**J**) PCR analysis to test the cleavage efficiency at *Myod1* locus in FISCs from mice injected with Ctrl/Single/Dual-sgRNA viruses. DNAs from C2C12 cells co-transfected with Cas9-expressing plasmid (pX458) and AAV9-dual sgMyod1 vector were used as positive control. Wild type (660 bp) and cleaved bands (~362 bp) are shown by arrowheads. (**K**) Left: SCs isolated from *Pax7*^{Cas9} mice administrated with middle dose of single/dual AAV9-sgMyod1 viruses were cultured for two days and IF stained for MYOD1. Right: the number of positively stained cells was counted. n = 6 mice per group. For each mouse, an average of 8 randomly selected fields were quantified. Scale bar, 50 μm. (**L**) Relative expressions of *Myod1* in the above SCs cultured for two or four days were determined by qRT-PCR (n = 3 to 5 mice per group). (**M**) Relative expression of *Myogenin* and *MyHC* in the above SCs cultured for two days were determined by qRT-PCR. n = 5 mice per group. (**N**) Schematic illustration to show non-homologous end joining (NHEJ) repair of double-strand breaks (DSBs) induced by AAV9-dual sgMyod1 (Guo et al., 2018). The edited products were divided into four groups based on whether the indels formed at either sgRNA or both target sites. Group I: editing at sgRNA2 site only; II: sgRNAc site only; III: individually at sgRNA2 and sgRNAc site; IV: simultaneously at both sites to cause deletion. (**O**) Distribution of the total sequencing reads in the dual sgRNAs group. About 27% of the total reads were detected as deletion. (**P**) The editing efficiency at sgRNA2 and sgRNAc sites in dual sgRNAs infected FISCs was determined by deep sequencing. SgRNA2 and sgRNAc yielded 86.2% and 70.21% indel formation respectively. The percentage was calculated as the ratio of the edited reads to the total reads. n=3 per group. All qRT-PCR data were normalized to *18S* or *Gapdh* mRNA. All the bar graphs are presented as mean ± s.d. *P<0.05, **P<0.01, ***P<0.001. ns, no significance.

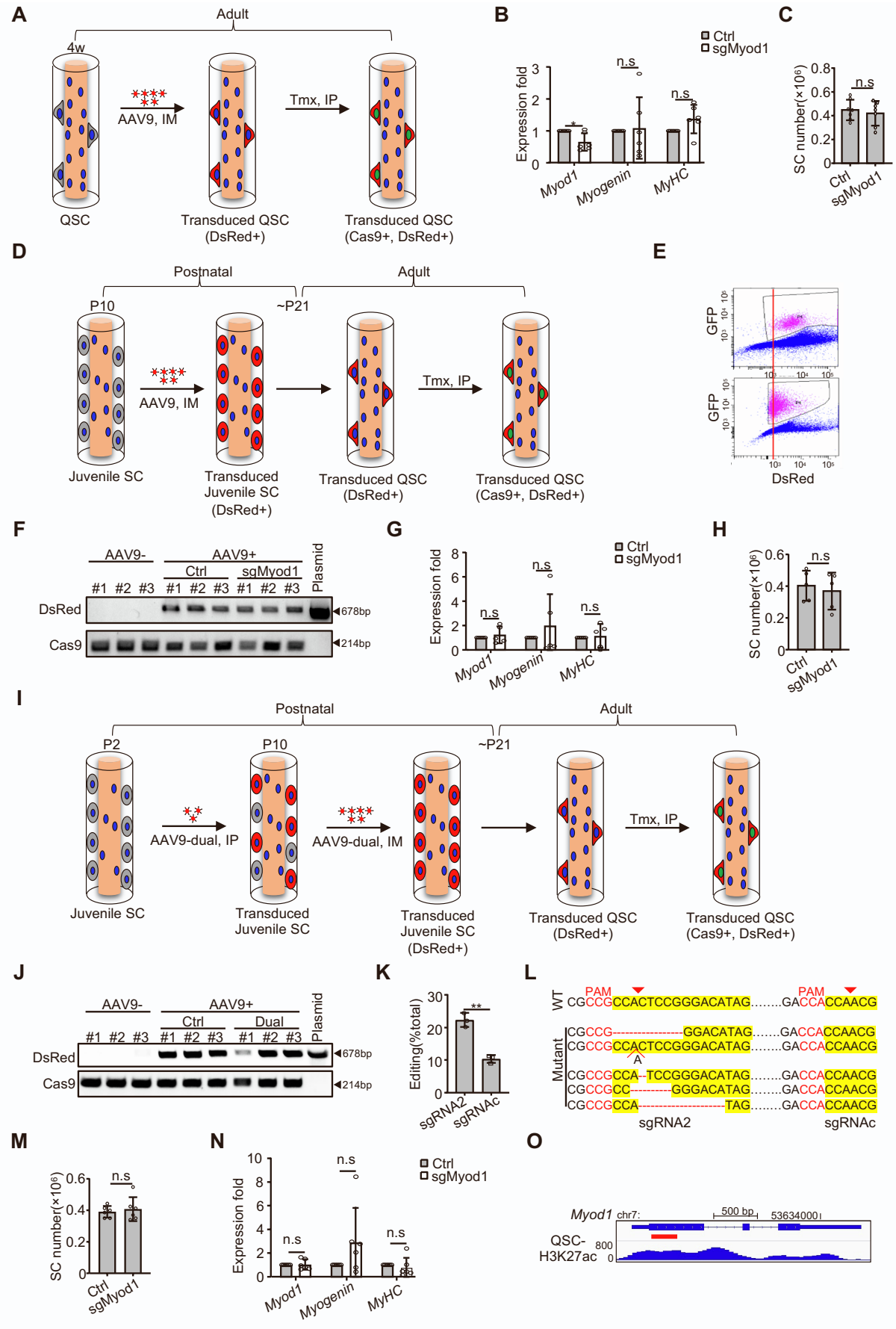
A
Adult
4w
AAV9, IM
Tmx, IP
QSC
Transduced QSC (DsRed+)
Transduced QSC (Cas9+, DsRed+)
B
Ctrl
sgMyod1
Expression fold
n.s
*
Myod1
Myogenin
MyHC
C
SC number(×10⁶)
n.s
Ctrl
sgMyod1
D
Postnatal
Adult
P10
~P21
AAV9, IM
Tmx, IP
Juvenile SC
Transduced Juvenile SC (DsRed+)
Transduced QSC (DsRed+)
Transduced QSC (Cas9+, DsRed+)
E
GFP
DsRed
F
AAV9-
AAV9+
Ctrl
sgMyod1
#1 #2 #3 #1 #2 #3 #1 #2 #3
Plasmid
DsRed
Cas9
678bp
214bp
G
Ctrl
sgMyod1
Expression fold
n.s
Myod1
Myogenin
MyHC
H
SC number(×10⁶)
n.s
Ctrl
sgMyod1
I
Postnatal
Adult
P2
P10
~P21
AAV9-dual, IP
AAV9-dual, IM
Tmx, IP
Juvenile SC
Transduced Juvenile SC
Transduced Juvenile SC (DsRed+)
Transduced QSC (DsRed+)
Transduced QSC (Cas9+, DsRed+)
J
AAV9-
AAV9+
Ctrl
Dual
#1 #2 #3 #1 #2 #3 #1 #2 #3
Plasmid
DsRed
Cas9
678bp
214bp
K
Editing(%total)
**
sgRNA2
sgRNAc
L
WT
PAM
CGCCGCCACTCCGGGACATAG.....GACCACCAACG
Mutant
CGCCG----------GGACATAG.....GACCACCAACG
CGCCGCCACTCCGGGACATAG.....GACCACCAACG
A
CGCCGCCA--TCCGGGACATAG.....GACCACCAACG
CGCCGCC---------GGGACATAG.....GACCACCAACG
CGCCGCCA----------TAG.....GACCACCAACG
sgRNA2
sgRNAc
M
SC number(×10⁶)
n.s
Ctrl
sgMyod1
N
Ctrl
sgMyod1
Expression fold
n.s
Myod1
Myogenin
MyHC
O
Myod1 chr7:
500 bp
53634000
QSC-H3K27ac
800
0

Figure S3. CRISPR/Cas9 fails to efficiently modify SCs at quiescent stage. Related to Figure 3. (**A**) Diagram to show the first strategy to edit QSCs. A high dose (5×10^{11} vg/mouse) of AAV9-sgMyod1 virus was intramuscularly (IM) injected into four-week-old *Pax7*$^{ER\text{-}Cas9}$ mice to transduce QSCs. Two weeks later, five consecutively intraperitoneal (IP) administrations of Tmx were conducted to induce Cas9 and GFP expression. The mice were sacrificed for SC isolation after another three weeks which provided enough time for possible editing. (**B**) Relative expressions of *Myod1*, *Myogenin* and *MyHC* mRNAs were detected in the SCs isolated from mice administrated in the first strategy (Figure 3B) and cultured for two days. n = 6 mice per group. (**C**) The number of SCs isolated from *Pax7*$^{ER\text{-}Cas9}$ mice in the first strategy. n = 7 mice per group. (**D**) Diagram to show the second strategy to edit QSCs. High dose of AAV9-sgMyod1virus was injected to *Pax7*$^{ER\text{-}Cas9}$ mice through IM at P10 to transduce proliferating juvenile SCs. Upon the termination of the postnatal myogenesis, a portion of the transduced cells were expected to become quiescence carrying the sgRNAs. Four weeks later, Tmx was injected via IP for five consecutive days to induce Cas9 and GFP expression and the mice were sacrificed for SC isolation and analysis after another three weeks. (**E**) Top: FACS plot showing the gating strategy to sort out Cas9-GFP positive SCs from *Pax7*$^{ER\text{-}Cas9}$ mice administrated in the second strategy (Figure 3G). A stronger DsRed signal compared to mice from Strategy 1 (bottom) indicates a higher transduction efficiency. (**F**) Genomic DNAs were isolated from FISCs of *Pax7*$^{ER\text{-}Cas9}$ mice in the second strategy and PCR was performed to amplify the DsRed or Cas9 coding region. Genomic DNAs from *Pax7*$^{ER\text{-}Cas9}$ mice without AAV9 administration were used as negative control and the AAV9-Myod1-sgRNA2 plasmid was used as positive control. n = 5 mice per group. (**G**) Relative expressions of *Myod1*, *Myogenin* and *MyHC* mRNAs were detected in the SCs isolated from the second strategy and cultured for two days. n = 5 mice per group. (**H**) The number of SCs isolated from *Pax7*$^{ER\text{-}Cas9}$ mice from the second strategy. n = 5 mice per group. (**I**) Diagram to show the third strategy to edit QSCs. A middle dose of AAV9-dual sgMyod1 virus was injected through IP into *Pax7*$^{ER\text{-}Cas9}$ mice at P2 and another high dose of the same virus was administrated at P10 through IM to transduce proliferating juvenile SCs, which was then followed by Tmx administration four weeks later to induce Cas9 and GFP expression. The mice were sacrificed for SC isolation after another three weeks. (**J**) Genomic DNAs were isolated from FISCs of *Pax7*$^{ER\text{-}Cas9}$ mice in the third strategy (Figure 3K) and PCR was performed to amplify the DsRed or Cas9 coding region. n = 6 mice per group. (**K**) Comparison of the editing efficiency between the sgRNA2 and sgRNAc sites. The editing efficiency at the two sites were markedly different (22.54% + 2.18% vs. 10.53% + 1.15%), possibly due to distinct accessibility to CRISPR/Cas9. n = 3 mice per group. (**L**) The five most frequently detected indel classes are shown with modifications occurring exclusively at the sgRNA2 target locus. (**M**) The number of SCs isolated from *Pax7*$^{ER\text{-}Cas9}$ mice in the third strategy. n = 6 mice per group. (**N**) Relative expressions of *Myod1*, *Myogenin* and *MyHC* mRNAs were detected in the above SCs cultured for four days. n = 6 mice per group. (**O**) Snapshot of H3K27ac ChIP-seq signal at *Myod1* locus in QSCs. The red bar indicates the targeted region. All qRT-PCR data were normalized to *18S* or *Gapdh* mRNA. All the bar graphs are presented as mean ± s.d. *P<0.05, **P<0.01. ns, no significance.

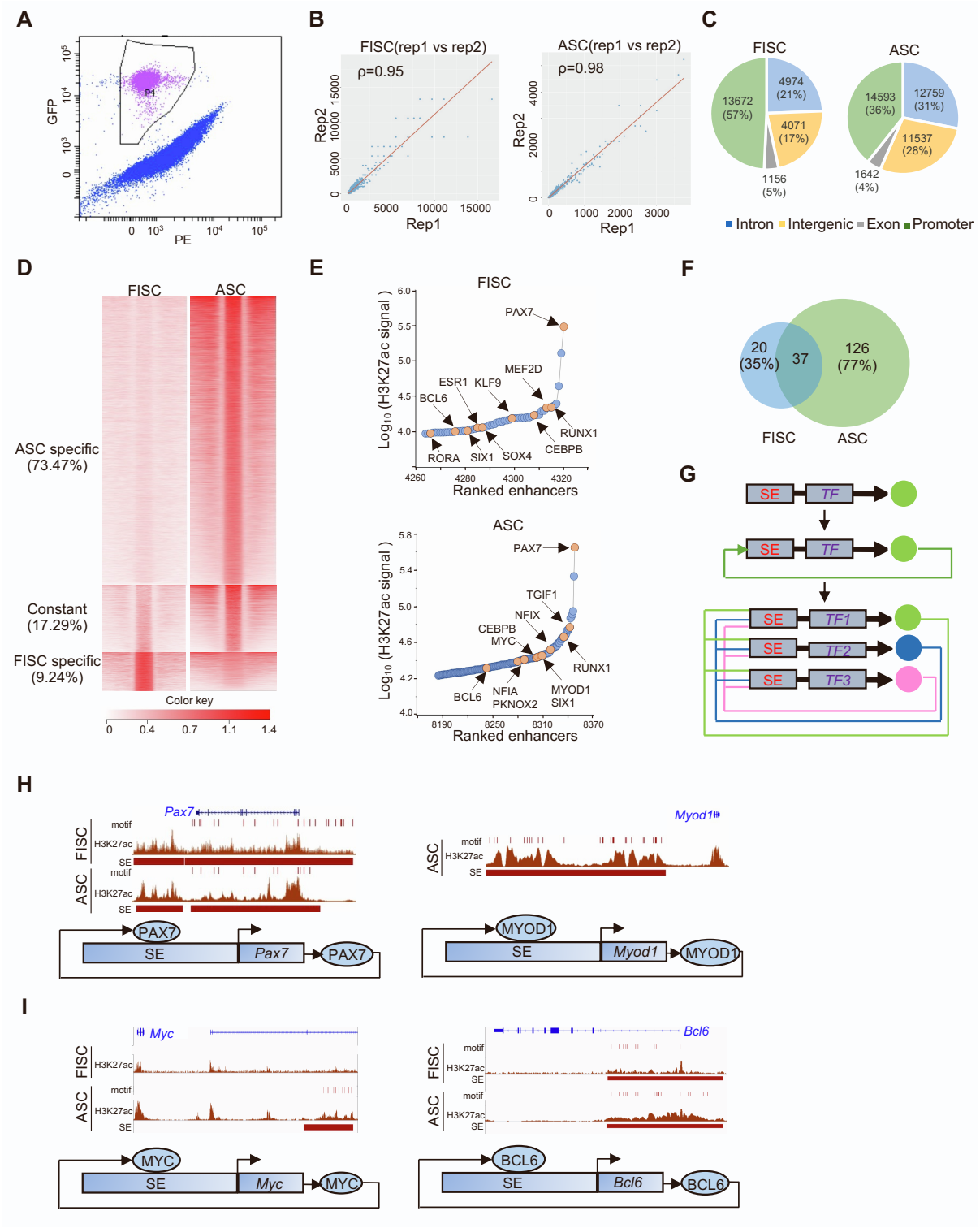

Figure S4. Key TFs regulating SC quiescence and activation are predicted through SEs. Related to Figure 4. (**A**) FACS plot showing the gating strategy for sorting out GFP positive SCs from *Pax7*-nGFP mice. (**B**) Reproducibility of two replicates of H3K27ac ChIP-seq datasets in FISCs or ASCs. (**C**) Genomic distribution of H3K27ac ChIP-seq reads in FISCs or ASCs. (**D**) Heatmaps of H3K27ac signals at ASC specific, constant, FISC specific enhancers. (**E**) Identification of SEs using ROSE in FISCs (Upper) and ASCs (Lower). Key TFs are shown. (**F**) Comparison of the SE landscapes between FISCs and ASCs. (**G**) Schematic illustration of the method to identify key TFs (Saint-André et

al., 2016). Cycles with various colors indicate different TFs. (**H**) Top: Genomic snapshots showing SEs associated with *Pax7* and *Myod1* loci. Bottom: illustration of auto-regulation of the above TFs and SEs. (**I**) Top: Genomic snapshots showing SEs associated with *Myc* and *Bcl6* loci. Bottom: illustration of auto-regulation of the above TFs and SEs.

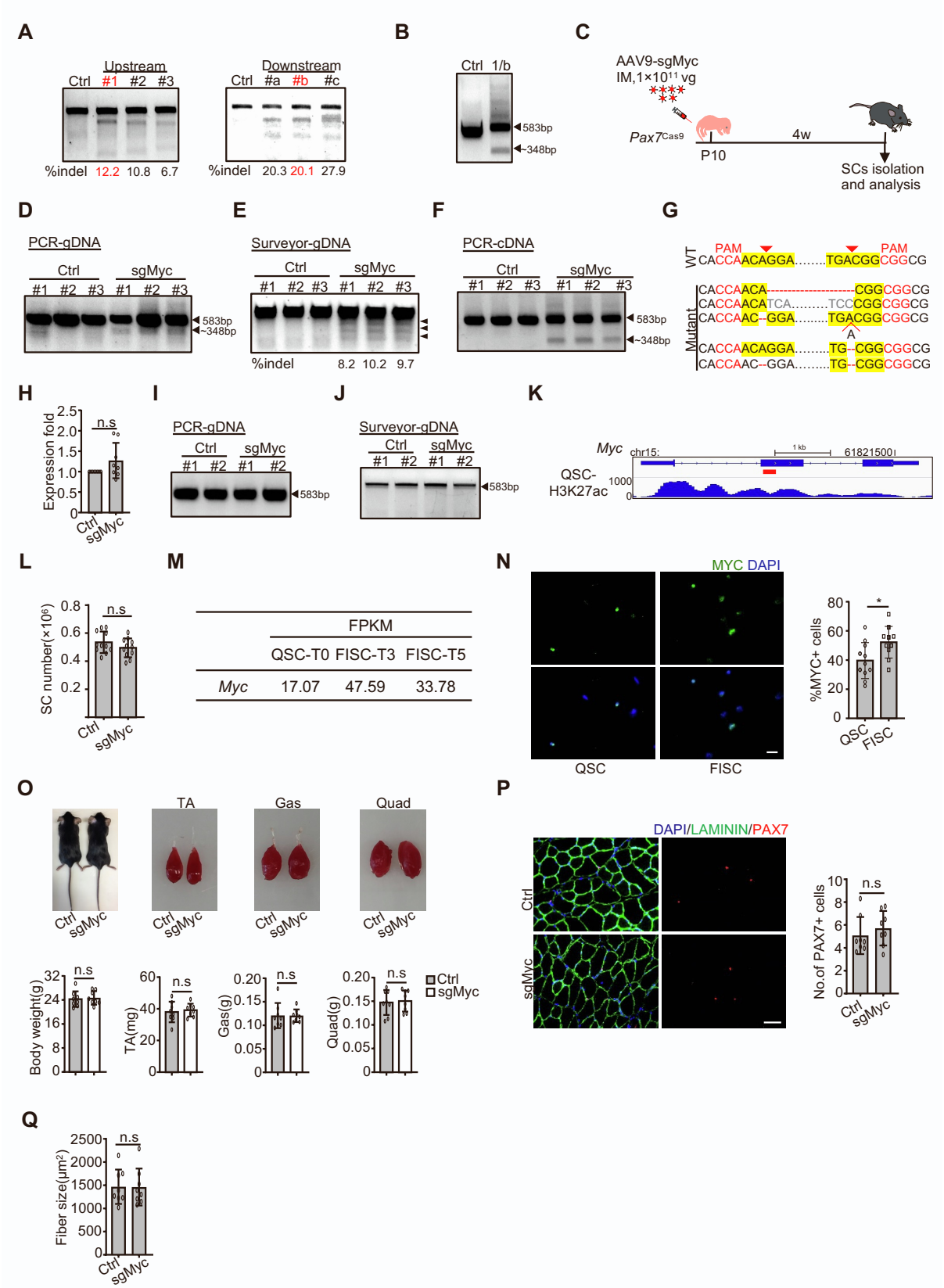

Figure S5. CRISPR/Cas9/AAV9-sgRNA mediated genome editing of *Myc* hinders SC activation and muscle regeneration. Related to Figure 5. (**A**) *In vitro* screening of sgRNAs targeting the up- and down-stream of *Myc* exon 2 in C2C12 cells. The frequency of indel occurrence is presented. SgRNA1 and sgRNAb which were expected to induce frameshift of *Myc* coding region were selected

for *in vivo* study and are marked in red. (**B**) Testing of the AAV9-dual sgMyc vector in C2C12 myoblasts. The above selected Myc-sgRNA1 and sgRNAb were cloned into the pAAV9-dual sgRNA vector sequentially and transfected into C2C12 cells together with a Cas9-expressing plasmid (pX458). Positively transfected cells were sorted out by GFP and DsRed one day after transfection and cultured for two days before PCR analysis to evaluate the deletion efficiency at *Myc* locus. Wild type (583 bp) and cleaved fragments (~348 bp) are indicated by arrowheads. (**C**) Schematic illustration of the experimental design for *in vivo* genome editing of *Myc* locus. *Pax7*^{Cas9} mice were intramuscularly administrated with middle dose of control or AAV9-dual sgMyc viruses at P10 and SCs were isolated four weeks later for analysis. **(D)** DNAs were isolated from the above FISCs and PCR was performed to test the cleavage efficiency. Wild type (583bp) and cleaved (~348bp) fragments are indicated by arrowheads. n = 3 mice per group. (**E**) The above genomic DNAs were subject to Surveyor assay to evaluate the editing efficiency at *Myc* locus. The arrowheads indicate the cleaved fragments by Surveyor. The frequency of indel occurrence is presented. n = 3 mice per group. (**F**) SCs isolated from *Pax7*^{Cas9} mice injected with high dose of AAV9-dual sgMyc viruses were cultured for 24 hrs and *Myc* cDNA was used for PCR analysis to test cleavage efficiency. Wild type (583bp) and cleaved (~348bp) fragments are indicated by arrowheads. (**G**) Representative sequencing reads for the AAV9-dual sgMyc targeted locus are shown. (**H**) The above SCs were cultured for 24 hrs and relative expression of *Myc* mRNAs was detected by qRT-PCR using *18S* mRNA as normalization. n = 8 mice per group. (**I**) The CRISPR/Cas9/AAV9-sgRNA system fails to modify *Myc* locus in QSCs. High dose of AAV9-dual sgMyc or control viruses were injected into *Pax7*$^{ER\text{-}Cas9}$ mice through IM at P10. Tamoxifen was injected intraperitoneally for five consecutive days to induce Cas9-GFP expression four weeks after AAV9 virus injection and the mice were sacrificed for SC isolation after another three weeks. Genomic DNAs from isolated SCs were subject to PCR analysis and a wild type band was amplified. n = 2 mice per group. (**J**) Surveyor nuclease assay was performed using the above DNA and no cleaved bands were detected. n = 2 mice per group. (**K**) Snapshot of H3K27ac ChIP-seq signal at *Myc* locus in QSCs. The red bar indicates the targeted region. (**L**) The number of SCs isolated from control or dual sgMyc virus treated mice. n = 11 mice per group. (**M**) Expression of *Myc* in QSCs or early activating FISCs was determined by RNA-seq (Machado et al., 2017). QSC-T0: SCs fixed by paraformaldehyde (PFA) before isolation. FISC-T3/5: SCs isolated by the standard 3 or 5-hour-long protocol. (**N**) IF staining of MYC in FISCs and QSCs (Left); the percentage of MYC positive cells was quantified from 11 randomly selected fields (Right). Scale bar, 20 μm. (**O**) *Pax7*^{Cas9} mice administrated with high dose of control or AAV9-dual sgMyc viruses did not show alteration in the weight of whole body or limb muscles. n = 8 mice per group. Representative images of mice and muscles are shown in the top. (**P**) Left: Immunostaining of PAX7 (red) and LAMININ (green) was performed on the uninjured TA muscle. Right: The number of PAX7 positive cells per 100 fibers was counted. n = 8 mice per group. For each mouse, an average of 17 randomly selected fields were quantified. (**Q**) Average fiber size of the uninjured TA muscle was quantified. n = 8 mice per group. Scale bar, 50 μm. All the bar graphs are presented as mean ± s.d. *P<0.05. ns, no significance.

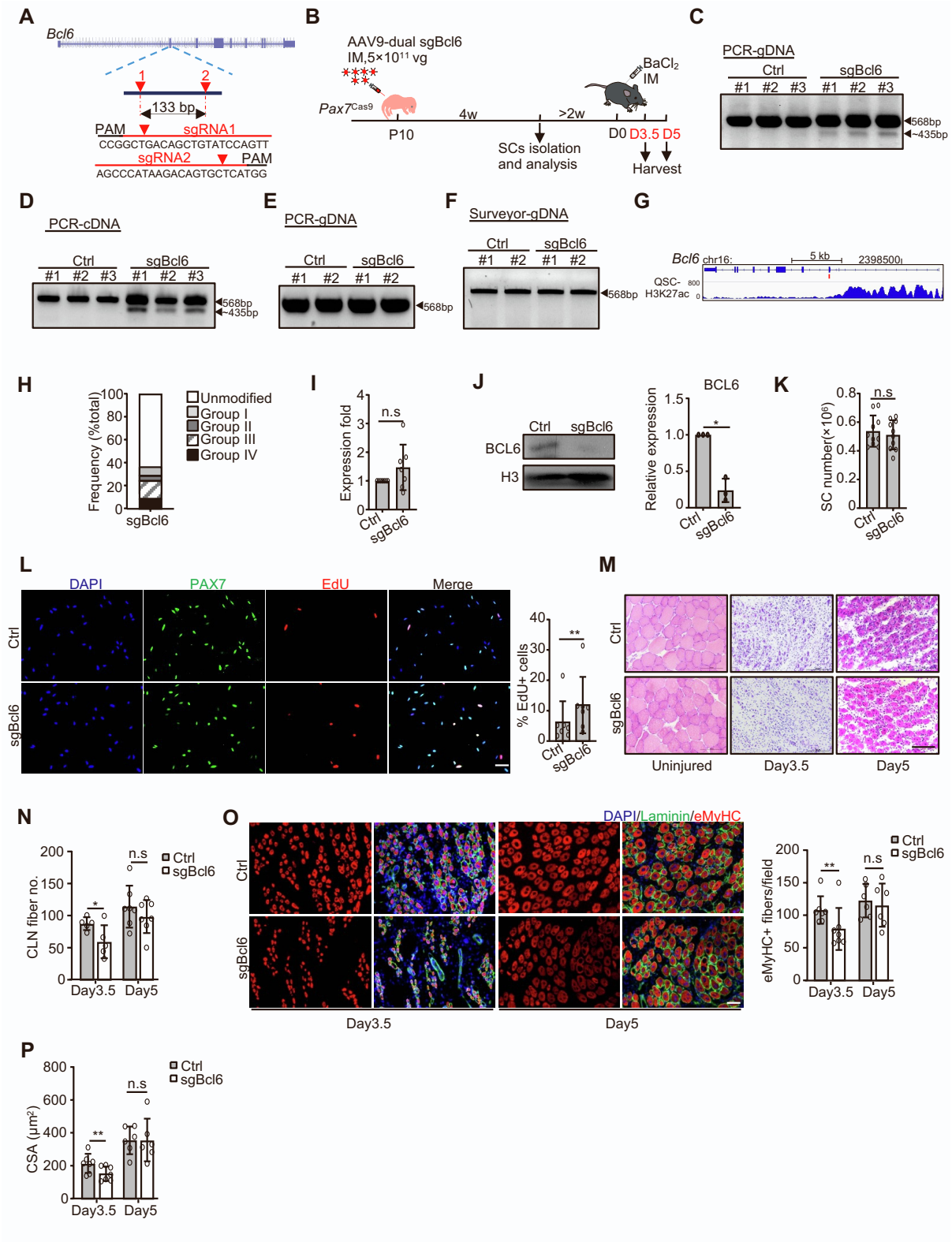

Figure S6. CRISPR/Cas9/AAV9-sgRNA mediated genome editing of *Bcl6* leads to abnormality of SC activation and muscle regeneration. Related to Figure 5. (**A**) Design of dual sgRNAs targeting *Bcl6* locus. SgRNA1 and sgRNA2 were designed to delete a 133 bp of exon 3. (**B**) Schematic illustration of the experimental design for *in vivo* genome editing of *Bcl6* locus followed by analysis of its effect on SCs and muscle regeneration. *Pax7*^{Cas9} mice were intramuscularly administrated with high dose of control or AAV9-dual sgBcl6 virus at P10 and SCs were isolated four weeks later for analyses.

To assay for muscle regeneration, $BaCl_2$ was intramuscularly injected into TA muscle at least six weeks after AAV9 virus administration (D0). The injected muscle was harvested 3.5 (D3.5) or 5 days (D5) post injury and subject to analysis. (**C**) Genomic DNAs were isolated from the above sorted SCs and PCR analysis was performed to test the cleavage efficiency. Wild type (568 bp) and cleaved (~435 bp) fragments are indicated by arrowheads. (**D**) SCs isolated from *Pax7*^{Cas9} mice injected with high dose of AAV9-dual sgBcl6 viruses were cultured for 24 hrs and Bcl6 cDNAs were used for PCR analysis to test cleavage efficiency. Wild type (568bp) and cleaved (~435bp) fragments are shown by arrowheads. (**E**) The CRISPR/Cas9/AAV9-sgRNA system fails to modify *Bcl6* locus in QSCs. High dose of AAV9-dual sgBcl6 or control viruses were injected into *Pax7*$^{ER\text{-}Cas9}$ mice through IM at P10. Tamoxifen was injected intraperitoneally for five consecutive days to induce Cas9-GFP expression four weeks after AAV9 virus injection and the mice were sacrificed for SC isolation after another three weeks. Genomic DNAs from isolated SCs were subject to PCR analysis and a wild type band was amplified. n = 2 mice per group. (**F**) Surveyor nuclease assay was performed using the above DNAs and no cleaved bands were detected. n = 2 mice per group. (**G**) Snapshot of H3K27ac ChIP-seq signal at *Bcl6* locus in QSCs. The red bar indicates the targeted region. (**H**) Distribution of the total sequencing reads for the AAV9-dual sgBcl6 targeted locus. Group I-IV were defined according to Figure S2N. (**I**) The above SCs were cultured for 24 hrs and relative expression of *Bcl6* mRNAs was detected by qRT-PCR. The qRT-PCR data were normalized to *18S* mRNA. n = 7 mice per group. (**J**) BCL6 protein level in the above SCs was examined by Western blot (Left) and the band intensity was quantified by Image J (Right). Histone H3 was used as loading control. n = 3 mice per group. (**K**) The number of SCs isolated from the above control or dual sgBcl6 virus treated mice. n = 10 mice per group. (**L**) The above FISCs were labeled with EdU for 24 hrs and the percentage of EdU positive cells was quantified. n = 7 mice per group. For each mouse, an average of 26 randomly selected fields were quantified. Scale bar, 50 μm. (**M-N**) H&E staining was performed 3.5 (D3.5) or 5 days (D5) post $BaCl_2$ injection (M) and the regenerating myofibers with CLN per field was quantified (N). n = 5 to 7 mice per group. For each mouse, an average of 6 randomly selected fields were quantified. Scale bar, 100 μm. (**O**) Immunostaining of eMyHC (red) and LAMININ (green) on the above TA muscle sections (Left) and the number of eMyHC+ myofibers was counted (Right). n = 6 to 7 mice per group. For each mouse, an average of 6 randomly selected fields were quantified. Scale bar, 50 μm. (**P**) The cross-sectional area (CSA) of the newly formed fibers with CLN was quantified. n = 6 to 7 mice per group. All the bar graphs are presented as mean ± s.d. *P<0.05, **P<0.01. ns, no significance.

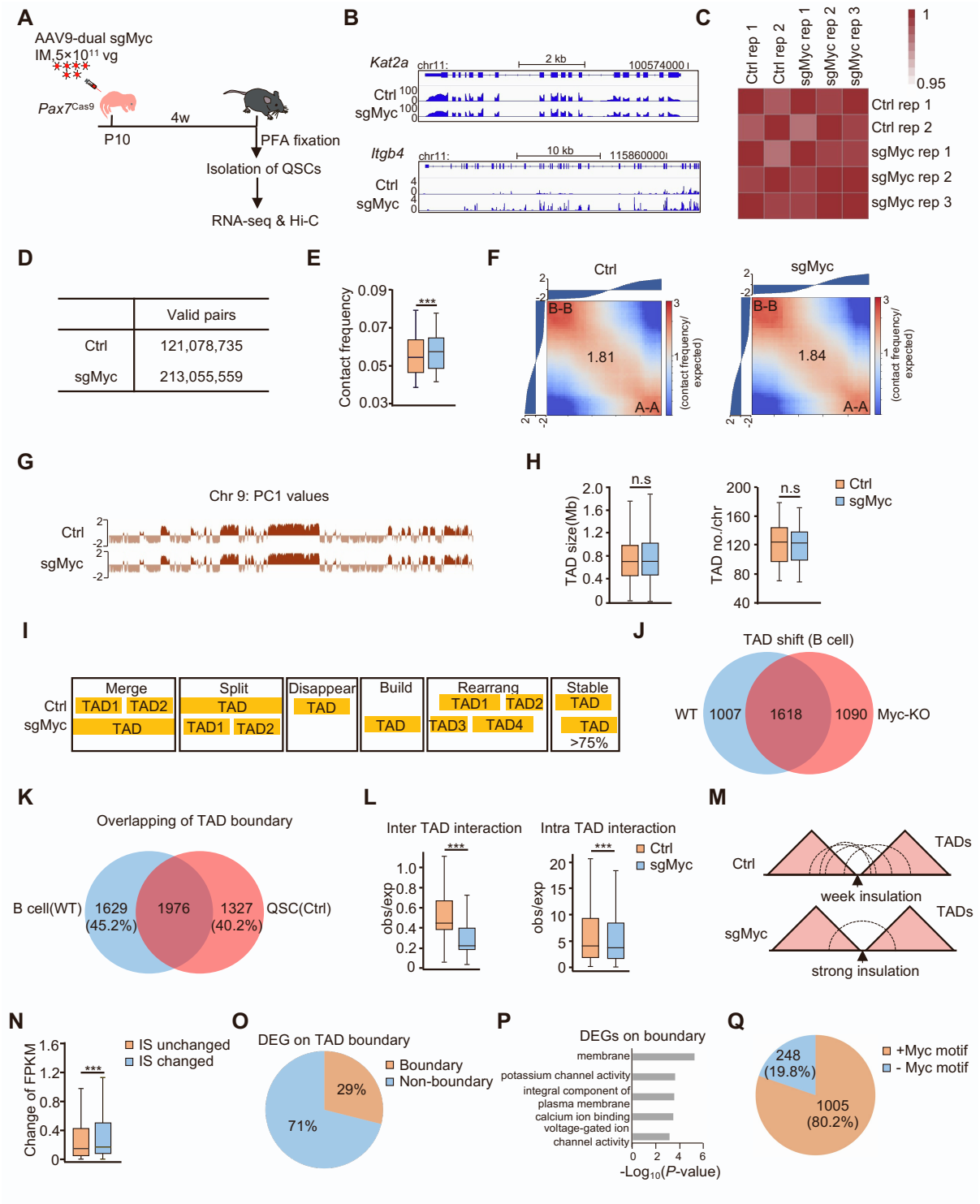

Figure S7. MYC orchestrates SC activation through impinging on 3D chromatin architecture. Related to Figure 6. (**A**) Schematic illustration of the experimental design to isolate Myc deficient QSCs for RNA-seq and Hi-C. *Pax7*^{Cas9} mice were intramuscularly administrated with high dose of control or AAV9-dual sgMyc viruses at P10 and SCs were isolated four weeks later. QSCs were isolated according to published protocol (Machado et al., 2017) using prior PFA fixation then subjected to RNA-seq and Hi-C experiment. (**B**) Genomic snapshots showing the expression of two known MYC regulated genes, *Kat2a* and *Itgb4*, in sgMyc vs. Ctrl. (**C**) Heatmap showing correlation between different groups and replicates (two biological replicates for control and three biological replicates for

sgMyc group) of the Hi-C experiments. (**D**) The number of valid pairs generated from Hi-C in each group. (**E**) Normalized interaction frequency for long-rang interactions (>5×10^{11} bp) in Ctrl and sgMyc QSCs**.** (**F**) Average contact frequency enrichment showing the extent of compartmentalization in Ctrl (Left) and sgMyc (Right) QSCs. (**G**) Distributions of PC1 values across entirety of chromosome 9 in Ctrl and sgMyc QSCs. The A compartments are shown in puce, and the B compartments are shown in beige. (**H**) Average TAD size (Left) and the number of TADs per chromosome (Right) in each group. (**I**) Illustration of TAD shift (Ke et al., 2017). If the overlapped portion of a given TAD in Ctrl and sgMyc group was over 0.75, it was defined as stable TAD, otherwise it was called rearranged TAD. If two or more TADs fused into one or on the contrary one divided into two or more TADs upon MYC depletion, the changes were named “merge” or “split” respectively. If one TAD was only identified in Ctrl or sgMyc QSCs, the changes were defined as “disappear” or “build”. TAD shift was defined when a TAD was split, merged, disappeared, built or rearranged upon MYC depletion. (**J**) Venn diagram showing the number of shifted TADs in WT vs Myc-KO B cells (Kieffer-Kwon et al., 2017). (**K**) Venn diagram showing the overlap of the TAD boundaries identified in WT B cells and Ctrl QSCs. (**L**) Boxplots showing inter- (Left) or intra-TAD (Right) interactions in Ctrl and sgMyc QSCs. Obs: observed; exp: expected. (**M**) Illustration of the change of IS upon MYC deletion (Stadhouders et al., 2018). (**N**) Boxplot showing the absolute FPKM changes for genes located within boundaries with at least 20% IS value change upon Myc depletion compared with those residing in IS unchanged boundaries. (**O**) Pie chart showing genomic distribution of DEGs within TAD boundary and non-boundary regions. (**P**) GO analysis of the DEGs resided within the boundaries was performed and the top five enriched items are shown in y axis. (**Q**) Pie chart showing the portion of TAD boundary located H3K27ac peaks containing MYC motif. Statistical analyses in **E**, **H**, **L** and **N** were done by Wilcoxon rank-sum test; ***P<0.001. ns, no significance.

Supplemental Experimental Procedures

Mice. *Pax7*-nGFP, *Pax7*^{Cre} and *Pax7*^{CreER} mice were kindly provided by Dr. Zhenguo Wu (Hong Kong University of Science & Technology). The Cre dependent *Rosa26*$^{Cas9\text{-}EGFP}$ knockin mice (B6;129-Gt (ROSA)26Sor$^{tm1(CAG\text{-}cas9*\text{-}EGFP)\ Fezh/J}$; stock number 024857) were obtained from the Jackson Laboratory. To generate Cas9 knockin mice, homozygous *Pax7*^{Cre} or *Pax7*^{CreER} mice were crossed with Rosa26$^{Cas9\text{-}EGFP}$ mice. For inducible Cas9 expression, Tamoxifen (100 mg/Kg body weight) was injected intraperitoneally into *Pax7*$^{ER\text{-}Cas9}$ mice for five consecutive days. Each mouse strain was genotyped by PCR using DNA extracted from mouse tail tissues. To induce acute injury, over 8-week-old mice were injected with 50 μL of 1.2% $BaCl_2$ (w/v in H_2O) solution into the tibialis anterior (TA) muscle. TA muscles were harvested at designated time points for further analysis. Primers used for genotyping are listed in Table S7.

Plasmids. To construct the AAV9-sgRNA transfer plasmids, the AAV: ITR-U6-sgRNA (backbone)-pCBh-Cre-WPRE-hGHpA-ITR (Addgene, 60229) was used as donor plasmid. Coding sequencing for DsRed was PCR-amplified and cloned into the donor plasmid through replacing the sequence encoding Cre using Age I and EcoR I sites. The CBh promoter was substituted with CMV promoter to drive DsRed expression. For single sgRNA expression system, sgRNA with the highest editing efficiency assessed by Surveyor nuclease assay was inserted into the AAV9-sgRNA vector (AAV: ITR-U6-sgRNA(backbone)-CMV-DsRed-WPRE- hGHpA-ITR) using Sap I site. To generate dual AAV-sgRNAs expression plasmid, the second sgRNA with good editing efficiency and targeting about 100 bp-300 bp away from the first sgRNA was constructed into the AAV9-sgRNA vector together with the gRNA cassette and U6 promoter using Xba I and Kpn I sites. To increase the editing efficiency, the two selected sgRNAs were designed to target 5' end of the coding region and the predicted deletion should cause frameshift of target gene. Primers for AAV9-sgRNA vector construction are listed in Table S7.

Cell culture. Mouse C2C12 myoblast cells (CRL-1772) and human HEK293FT cells were obtained from ATCC and cultured in DMEM with 10% FBS, 100 units/ml penicillin, 100 μg/ml streptomycin and 2 mM L-glutamine (GM, growth medium) in 5% CO_2 at 37 ◦C.

Satellite cell isolation, culture and EdU incorporation assay. Isolated satellite cells were cultured in growth medium (F10 medium (Merck Millipore) supplemented with 20% FBS, 1% penicillin/streptomycin and 5 ng/mL basic fibroblast growth factor (bFGF)) at 37◦C in 5% CO_2. To induce spontaneous differentiation, satellite cells were cultured in growth medium up to four days. For EdU incorporation assay, EdU was added to the SC culture medium with a final concentration of 10 mM and the incorporation assay was detected by Click-iT EdU kit (Invitrogen) according to the manufacturer's instructions.

SgRNA design, selection and Surveyor nuclease assay. In brief, site specific sgRNAs were predicted following a web tool Crispor (Haeussler et al., 2016) (http://crispor.tefor.net/). To minimize off-target effects, only sgRNAs with a score higher than 5 were selected. To determine the editing efficiency, annealed oligonucleotides were constructed into a Cas9-EGFP expressing vector (pX458, Addgene) using Bbs I site. SgRNA-pX458 plasmids were transiently transfected into C2C12 using

Lipofectamine 3000. GFP positive cells were sorted out using FACS 48 hrs after transfection and cultured for another two days. Genomic DNAs were extracted by QuickExtract (Epicentre) solution and amplified by Phusion High-Fidelity DNA Polymerase (NEB) using primers against the edited locus. Purified PCR products were subject to Surveyor nuclease assay (Integrated DNA Technologies) according to the manufacturer's protocol (Ran et al., 2013). Briefly, 360 ng of DNA was denatured at 95°C and re-annealed to form hetero-duplexes. The resulting product was digested by Surveyor Nuclease S at 42 °C for 30 minutes and separated on a 2% agarose gel. The percentage of indel formation was determined by relative band intensities. The band intensity of the gel was first evaluated by Image J. The percentage of the PCR product cleaved (f_{cut}) for each lane was then calculated using the formula: f_{cut} = (b + c)/ (a + b + c), where a is the integrated intensity of the undigested PCR product and b and c are the integrated intensities of each cleavage product. The percentage of indel was then estimated by the formula: indel (%) = 100 × (1-$\sqrt{(1-fcut)}$). For the control group, genomic DNA from C2C12 cells transfected with Cas9-EGFP expressing plasmid (pX458) without any sgRNA insertion was used and subjected to Surveyor nuclear assay. Sequences for sgRNAs and primers used for Surveyor assay are listed in Table S7.

AAV9 virus production, purification and injection. AAV9 serotype plasmid and pDF6 are kind gifts from Dr. Bin Zhou (Yu et al., 2016). AAV9 virus particles were produced in HEK293FT cells by the triple transfection method (Grieger et al., 2006). In brief, HEK293FT cells were seeded in T75 flask and transiently transfected with AAV9-sgRNA vector (5 μg), AAV9 serotype plasmid (5 μg), and pDF6 (AAV helper plasmid) (10 μg) at a ratio of 1:1:2 using polyethyleneimine (PEI) when the cell reached 80%~90% confluent. Twenty-four hrs after transfection, the cells were changed to growth medium (DMEM with 10% FBS, 100 units/ml penicillin, 100 μg/ml streptomycin and 2 mM L-glutamine) and cultured for another forty-eight hrs. The cells were harvested by Trypsin-EDTA (Gibco) and washed with PBS for two times. To release the AAV9 virus, the pellet was re-suspended with lysis buffer (Tris-HCl, PH 8.0, 50 mM; NaCl, 150 mM) followed by three sequential freeze–thaw cycles (liquid nitrogen/37°C). The lysate was treated with Benzonase (Sigma) together with $MgCl_2$ (final concentration: 1.6 mM) at 37°C for 0.5~1 hr followed by centrifugation at 3,000 rpm for 10 minutes. The supernatant was filtered with 0.45 μm sterile filter and added with equal volume of 1 M NaCl and 20% PEG8000 (w/v) to precipitate the virus at 4 °C overnight. After centrifugation at 12,000 g for 30 minutes at 4 °C, the supernatant was remove and the pellet was re-suspended with sterile PBS and then subject to centrifugation at 3,000 g for 10 minutes. Equal volume of chloroform was then added and shaken. The mixture was spun down at 12,000 g for 15 minutes at 4 °C. The aqueous layer was filtered by 0.22 μm sterile filter and passed through a 100 kDa MWCO (Millipore). The concentrated solution was washed with sterile PBS for three times. The tilter of the AAV9 virus was determined by qRT-PCR using primers targeting the CMV promoter. For AAV9 administration, 50-100 μL of AAV9-sgRNA (high dose: 5×10^{11} vg; middle dose: 1×10^{11} vg; low dose: 0.2×10^{11} vg) or control (AAV9-sgRNA vector without sgRNAs insertion) virus was diluted in saline and injected systemically through intraperitoneal (IP) injection on postnatal day 2 (P2) or locally to the skeletal muscles through intramuscular (IM) injection on P10. All the used primers are listed in Table S7.

Immunoblotting, immunostaining and immunohistochemistry. Tissue samples were homogenized in 400 μl of ice cold RIPA buffer supplemented with protease inhibitors cocktail (Sigma-Aldrich) and lysed on ice for 40 minutes. Total cell extracts for Western blot were prepared as described previously

(Lu et al., 2013; Zhou et al., 2015). Following antibodies were used: MYOD1 (Dako, M3512, 1:2000), α-TUBULIN (Santa Cruz Biotechnology, sc-23948, 1:2000), Cas9 (Cell Signaling Technology, #14697, 1:1000), PAX7 (Developmental Studies Hybridoma Bank; 1:1000), GFP (Santa Cruz Biotechnology, sc-8334, 1:1000), GAPDH (Santa Cruz Biotechnology, sc-137179, 1:2000), Histone H3 (Santa Cruz Biotechnology, sc-517576, 1:3000), MYC (Santa Cruz Biotechnology, sc-40, 1:1000), BCL6 (Santa Cruz Biotechnology, sc-365618/sc-7388, 1:500), MYOGENIN (Santa Cruz Biotechnology, sc-576, 1:1000). For immunofluorescence staining, following antibodies and related dilutions were used: MYOD1 (Dako, M3512, 1:800), PAX7 (Developmental Studies Hybridoma Bank; 1:100), DsRed (Santa Cruz Biotechnology, sc-390909, 1:400), MYC (Santa Cruz Biotechnology, sc-40, 1:500). Hematoxylin and eosin (H&E) staining on frozen muscle sections was performed as described previously (Diao et al., 2012). Immunofluorescence staining on frozen muscle sections was performed using the following antibodies: Laminin (Sigma, L9393, 1:800), eMyHC (Sigma, 1:200), PAX7 (Developmental Studies Hybridoma Bank; 1:50). All fluorescent images were captured with a fluorescence microscope (Leica DM6000B).

qRT-PCR. Total RNAs from cells were extracted using TRIzol reagent (Life Technologies) according to the manufacturer's instructions and cDNAs were prepared using PrimeScript™ RT Master Mix kit (Takara, RR036A). Analysis of mRNA expression was performed with SYBR Green Master Mix (Life Technologies) on a 7900HT System (Life Technologies). All the used primers are listed in Table S7.

RNA-seq and data analysis. RNA-seq was performed as described previously (Zhao et al., 2019). Total RNAs were extracted from PFA fixated, freshly isolated or cultured SCs and subject to poly(A) selection (Ambion, 61006) followed by library preparation using NEBNext® Ultra™ II RNA Library Preparation Kit (NEB). Libraries with barcodes were pooled at equal concentrations and sequenced on the Illumina HiSeq 1500 platform. For data analysis, sequenced reads were mapped to reference mouse genome using TopHat (v2.0.13). Cufflinks (v2.1.1) was then employed to estimate transcript abundance. Abundance was reported in Fragments Per Kilobase per Million (FPKM). Differentially expressed genes were identified if the change of expression level exceeds a fold change threshold (> 2).

ChIP-seq and data analysis. ChIP-seq and the data analysis were performed following the procedures described in our previous studies (Chen et al., 2019; Peng et al., 2017). In brief, chromatins from freshly isolated or cultured SCs were fragmented using sonicator and incubated with 5 μg antibody against histone H3-K27 acetylation (Abcam, ab4729, rabbit poly-clonal) overnight at 4 °C. The purified DNA (200 ng) was subject to library preparation using NEBNext® Ultra™ II DNA Library Preparation Kit (NEB). Libraries with barcodes were pooled and sequenced on the Illumina HiSeq 1500 platform. For data analysis, a standard approach was used to conduct base calling and convert the results into raw reads in FASTQ format. After adapter trimming and quality filtering, reads were first aligned to mm9 reference genome by Bowtie2 with default parameters, then removed duplication and called enriched regions (peaks) by MACS2 with q-value equal to 0.01. Annotation of enhancers and super enhancers was performed as described before with minor adjustment (Peng et al., 2017). Enriched H3K27ac regions(peaks) were identified by MACS2 using merged bam files from all replicates at each stage with q-value 0.01. Peaks were subject to a filter to exclude the ENCODE blacklisted regions as well as those within +/-2 kb of a Refseq Transcription Start Site (TSS) and the

filtered peaks were defined as enhancers. For super enhancer identification, unlike ROSE (Whyte et al., 2013) pipeline in which enhancers within 12.5 kb of each other are combined into stitched enhancer regions and then assigned to nearby genes, in our prediction, enhancers were first assigned to expressed genes (RPKM >0.5) whose TSSs are nearest to the center of the enhancer region; then the enhancers assigned to the same genes and within 12.5 kb of one another were stitched together and further subject to super enhancer identification using the ROSE algorithm. SE constituents were extended by 500 bp on both side and used as input regions to scan motifs for transcription factors by FIMO with default parameters. The Position weight matrix (PWM) of the motifs were obtained from the TRANSFAC database. For key TF prediction, if its DNA binding motif was predicted in its own SE region for at least three times, this kind of SE associated TFs was assigned as auto-regulated TFs; key TFs were defined as auto-regulated TFs whose binding motifs were predicted in the SE regions of other auto-regulated TFs.

Hi-C and data analysis. The *in situ* Hi-C libraries were prepared as previously reported (Ke et al., 2017; Rao et al., 2014; Stadhouders et al., 2018). Briefly, isolated SCs were digested using 100U DpnII overnight at 37 °C and then filled in with biotin for 1.5 hours at 37 °C; ligated for 4.5 hours at room temperature. DNA was purified by ethanol precipitation, and then sheared into 300-400bp fragments using Covaris S220. DNA fragments containing biotin were enriched by Dynabeads MyOne Streptavidin C1 (Invitrogen 65001) for 15 min at room temperature, followed by end repairing, adaptor ligation and PCR amplification as described (Rao et al., 2014). At least two biological replicates were performed for both control and sgMyc groups. The libraries were then sequenced via the Illumina HiSeq X Ten system at Genewiz company.

The *in-situ* Hi-C data was processed following a standard pipeline Hi-C-Pro (Servant et al., 2015). Briefly, the reads were aligned to reference genome (mm9) in two steps: global alignment was first performed for all pair-end reads; unaligned reads were then trimmed by restriction enzyme and aligned again. All aligned reads were then merged together to assign to restriction fragments. In this step, invalid fragments (dangling end, self-cycle etc.) were discarded and PCR duplications were removed for each biological replicate separately. At last, all validate pairs were normalized by read depth using HOMER (Heinz et al., 2010) followed by ICE matrix balancing (Imakaev et al., 2012) to further get interaction matrix.

To separate the genome into A/B compartments, ICE normalized Hi-C matrices at 100-kb resolution were split into chromosomal matrices and Pearson correlation was applied in the transformed correlation matrices. The annotation of genes including the expression profile was used to assign negative and positive PC1 categories to each compartment. The compartmentalization strength was measured using cool tools (https://github.com/mirnylab/cooltools). Basically, all compartment bins were divided into 50 degrees based on the ranking of PC1 value, and then the average interaction strength (observed/expected) between each degree was calculated to obtain the saddle plot. The compartmentalization score was calculated using top 20% of intra-compartment divided by top 20% of inter-compartment based on PC1 value.

TopDom (Shin et al., 2016) was applied to identify TADs. Briefly, TopDom first computed a score by calculating the average interaction frequency around a distinct window of each bin and then identified TAD boundary under statistical testing as the local minimal signal within certain distance. Normalized contact matrices at 40 kb resolution were used for TAD identification. The unaltered TADs were defined following two criteria: 1) The distance of both TAD boundaries between two conditions

was less than or equal to 40 kb; 2) The overlapping between two TADs should be larger than 75% to exclude TADs with small size. The insulation index for each bin was generated based on a previously described method (Crane et al., 2015) by calculating the number of interactions across a specific bin on each side. The insulation score of the identified TAD border was defined through the same method (Crane et al., 2015), which used the local maximum on the outside of TAD to minus the local minimum of the inside of TAD of each boundary bin.

Deep-seq. Deep-seq was performed as previously described (Guo et al., 2018, 2017; Johansen et al., 2017). Briefly, genomic DNAs from AAV9-sgRNA infected SCs were amplified using Q5 High-Fidelity 2× Master Mix (NEB). PCR products were purified through QIAQuick PCR purification kit (Qiagen) and subject to library preparation using NEBNext® Ultra™ II DNA Library Preparation Kit (NEB). Libraries with barcodes were pooled and sequenced on the Illumina HiSeq 1500 platform. For data analysis, an online tool CRISPResso2 (http://crispresso.pinellolab.partners.org/) (Clement et al., 2019) was employed to calculate the indel occurrence. Primers used for Deep-seq are listed in Table S7.

Supplemental References

Chen, F., Zhou, J., Li, Y., Zhao, Y., Yuan, J., Cao, Y., Wang, L., Zhang, Z., Zhang, B., Wang, C.C., et al. (2019). YY1 regulates skeletal muscle regeneration through controlling metabolic reprogramming of satellite cells. The EMBO Journal *38*, e99727.

Clement, K., Rees, H., Canver, M.C., Gehrke, J.M., Farouni, R., Hsu, J.Y., Cole, M.A., Liu, D.R., Joung, J.K., Bauer, D.E., et al. (2019). CRISPResso2 provides accurate and rapid genome editing sequence analysis. Nature Biotechnology *37*, 224–226.

Crane, E., Bian, Q., McCord, R.P., Lajoie, B.R., Wheeler, B.S., Ralston, E.J., Uzawa, S., Dekker, J., and Meyer, B.J. (2015). Condensin-driven remodelling of X chromosome topology during dosage compensation. Nature *523*, 240–244.

Diao, Y., Guo, X., Li, Y., Sun, K., Lu, L., Jiang, L., Fu, X., Zhu, H., Sun, H., Wang, H., et al. (2012). Pax3/7BP Is a Pax7- and Pax3-Binding Protein that Regulates the Proliferation of Muscle Precursor Cells by an Epigenetic Mechanism. Cell Stem Cell *11*, 231–241.

Grieger, J.C., Choi, V.W., and Samulski, R.J. (2006). Production and characterization of adeno-associated viral vectors. Nature Protocols *1*, 1412–1428.

Guo, T., Feng, Y.-L., Xiao, J.-J., Liu, Q., Sun, X.-N., Xiang, J.-F., Kong, N., Liu, S.-C., Chen, G.-Q., Wang, Y., et al. (2018). Harnessing accurate non-homologous end joining for efficient precise deletion in CRISPR/Cas9-mediated genome editing. Genome Biology *19*, 170.

Guo, Y., VanDusen, N.J., Zhang, L., Gu, W., Sethi, I., Guatimosim, S., Ma, Q., Jardin, B.D., Ai, Y., and Zhang, D. (2017). Analysis of cardiac myocyte maturation using CASAAV, a platform for rapid dissection of cardiac myocyte gene function in vivo. Circulation Research *120*, 1874–1888.

Haeussler, M., Schönig, K., Eckert, H., Eschstruth, A., Mianné, J., Renaud, J.-B., Schneider-Maunoury, S., Shkumatava, A., Teboul, L., and Kent, J. (2016). Evaluation of off-target and on-target scoring algorithms and integration into the guide RNA selection tool CRISPOR. Genome Biology *17*, 148.

Heinz, S., Benner, C., Spann, N., Bertolino, E., Lin, Y.C., Laslo, P., Cheng, J.X., Murre, C., Singh, H., and Glass, C.K. (2010). Simple Combinations of Lineage-Determining Transcription Factors Prime cis-Regulatory Elements Required for Macrophage and B Cell Identities. Molecular Cell *38*, 576–589.

Imakaev, M., Fudenberg, G., McCord, R.P., Naumova, N., Goloborodko, A., Lajoie, B.R., Dekker, J., and Mirny, L.A. (2012). Iterative correction of Hi-C data reveals hallmarks of chromosome organization. Nature Methods *9*, 999–1003.

Johansen, A.K., Molenaar, B., Versteeg, D., Leitoguinho, A.R., Demkes, C., Spanjaard, B., de Ruiter, H., Akbari Moqadam, F., Kooijman, L., and Zentilin, L. (2017). Postnatal cardiac gene editing using CRISPR/Cas9 with AAV9-mediated delivery of short guide RNAs results in mosaic gene disruption. Circulation Research *121*, 1168–1181.

Ke, Y., Xu, Y., Chen, X., Feng, S., Liu, Z., Sun, Y., Yao, X., Li, F., Zhu, W., and Gao, L. (2017). 3D chromatin structures of mature gametes and structural reprogramming during mammalian embryogenesis. Cell *170*, 367-381. e20.

Kieffer-Kwon, K.-R., Nimura, K., Rao, S.S.P., Xu, J., Jung, S., Pekowska, A., Dose, M., Stevens, E., Mathe, E., Dong, P., et al. (2017). Myc Regulates Chromatin Decompaction and Nuclear Architecture during B Cell Activation. Molecular Cell *67*, 566-578.e10.

Lu, L., Sun, K., Chen, X., Zhao, Y., Wang, L., Zhou, L., Sun, H., and Wang, H. (2013). Genome-wide survey by ChIP-seq reveals YY1 regulation of lincRNAs in skeletal myogenesis. The EMBO Journal *32*, 2575–2588.

Machado, L., de Lima, J.E., Fabre, O., Proux, C., Legendre, R., Szegedi, A., Varet, H., Ingerslev, L.R., Barrès, R., and Relaix, F. (2017). In situ fixation redefines quiescence and early activation of skeletal muscle stem cells. Cell Reports *21*, 1982–1993.

van Overbeek, M., Capurso, D., Carter, M.M., Thompson, M.S., Frias, E., Russ, C., Reece-Hoyes, J.S., Nye, C., Gradia, S., and Vidal, B. (2016). DNA repair profiling reveals nonrandom outcomes at Cas9-mediated breaks. Molecular Cell *63*, 633–646.

Peng, X.L., So, K.K., He, L., Zhao, Y., Zhou, J., Li, Y., Yao, M., Xu, B., Zhang, S., and Yao, H. (2017). MyoD-and FoxO3-mediated hotspot interaction orchestrates super-enhancer activity during myogenic differentiation. Nucleic Acids Research *45*, 8785–8805.

Ran, F.A., Hsu, P.D., Wright, J., Agarwala, V., Scott, D.A., and Zhang, F. (2013). Genome engineering using the CRISPR-Cas9 system. Nature Protocols *8*, 2281–2308.

Rao, S.S.P., Huntley, M.H., Durand, N.C., Stamenova, E.K., Bochkov, I.D., Robinson, J.T., Sanborn, A.L., Machol, I., Omer, A.D., Lander, E.S., et al. (2014). A 3D Map of the Human Genome at Kilobase Resolution Reveals Principles of Chromatin Looping. Cell *159*, 1665–1680.

Saint-André, V., Federation, A.J., Lin, C.Y., Abraham, B.J., Reddy, J., Lee, T.I., Bradner, J.E., and Young, R.A. (2016). Models of human core transcriptional regulatory circuitries. Genome Res. *26*, 385–396.

Servant, N., Varoquaux, N., Lajoie, B.R., Viara, E., Chen, C.-J., Vert, J.-P., Heard, E., Dekker, J., and Barillot, E. (2015). HiC-Pro: an optimized and flexible pipeline for Hi-C data processing. Genome Biol *16*, 259.

Shin, H., Shi, Y., Dai, C., Tjong, H., Gong, K., Alber, F., and Zhou, X.J. (2016). TopDom: an efficient and deterministic method for identifying topological domains in genomes. Nucleic Acids Res *44*, e70–e70.

Stadhouders, R., Vidal, E., Serra, F., Di Stefano, B., Le Dily, F., Quilez, J., Gomez, A., Collombet, S., Berenguer, C., Cuartero, Y., et al. (2018). Transcription factors orchestrate dynamic interplay between genome topology and gene regulation during cell reprogramming. Nature Genetics *50*, 238–249.

Whyte, W.A., Orlando, D.A., Hnisz, D., Abraham, B.J., Lin, C.Y., Kagey, M.H., Rahl, P.B., Lee, T.I., and Young, R.A. (2013). Master transcription factors and mediator establish super-enhancers at key cell identity genes. Cell *153*, 307–319.

Yu, W., Huang, X., Tian, X., Zhang, H., He, L., Wang, Y., Nie, Y., Hu, S., Lin, Z., Zhou, B., et al. (2016). GATA4 regulates Fgf16 to promote heart repair after injury. Development *143*, 936.

Zhao, Y., Zhou, J., He, L., Li, Y., Yuan, J., Sun, K., Chen, X., Bao, X., Esteban, M.A., Sun, H., et al. (2019). MyoD induced enhancer RNA interacts with hnRNPL to activate target gene transcription during myogenic differentiation. Nature Communications *10*, 5787.

Zhou, L., Sun, K., Zhao, Y.U., Zhang, S., Wang, X., Li, Y., Lu, L., Chen, X., Chen, F., and Bao, X. (2015). Linc-YY1 promotes myogenic differentiation and muscle regeneration through an interaction with the transcription factor YY1. Nature Communications *6*, 1–16.